pH-Induced Conformational Transition in the Soluble CuA Domain of *Paracoccus denitrificans* Cytochrome Oxidase†

Sayan Gupta,‡ Antony Warne,§ Matti Saraste,§ and Shyamalava Mazumdar*,‡

Department of Chemical Sciences, Tata Institute of Fundamental Research, Homi Bhabha Road, Colaba, Mumbai 400005, India, and European Molecular Biology Laboratory, Postfach 10 2209, Meyerhofstrasse 1, 6900 Heidelberg, Germany

Received September 20, 2000; Revised Manuscript Received February 6, 2001

ABSTRACT: The pH-induced conformational transition in the CuA domain of subunit II of cytochrome oxidase of *Paracoccus denitrificans* (PdII) has been investigated using various spectroscopic and stopped-flow kinetic methods. UV−visible absorption and circular dichroism studies showed that an increase in pH from 6 to 10 leads to a conformation change with pK_a = 8.2 associated with the CuA site of the protein. The secondary structure of the protein was, however, shown to remain unchanged in these two conformational states. Thermal and urea-induced unfolding studies showed that the "low-pH" conformation is more stable compared to the "high-pH" conformation of the protein. Moreover, the overall stability of the protein was found to decrease on reduction of the metal centers in the low-pH form, while the oxidation state of the metal centers did not have any significant effect on the overall stability of the protein in the high-pH form. Stopped-flow pH-jump kinetic studies suggested that the conformational transition is associated with a slow deprotonation step followed by fast conformational equilibrium. The results are discussed in the light of understanding the pH-induced conformational change in the β-barrel structure of the protein and its effect on the coordination geometry of the metal site.

The type IIIA purple binuclear copper center (CuA) forms the electron entry site of cytochrome *c* oxidase (CcO) (*1*−*3*). Recent crystallographic and other studies showed that the structure of this site is highly conserved in the CcO of eukaryotic mitochrondria (*4*, *5*), of aerobic bacteria (*6*−*9*), and in the nitrous oxide reductase (N_2OR) of denitrifying bacteria (*10*). This site is situated at the solvent-exposed part of the subunit II of the enzyme and accepts electrons from cytochrome *c*. Subsequently, it transfers the electrons to the heme *a* in subunit I of the enzyme in the terminal stage of respiratory electron transfer, leading to reduction of molecular oxygen to water at the binuclear heme a_3−CuB catalytic center (*1*−*3*). The biochemical properties of the CuA site thus involve long-range electron transfer analogous to that of type I copper proteins such as azurin in denitrifying bacteria (*11*). However, unlike the blue copper proteins that contain (*11*) a mononuclear Cu(II) with one cysteine and two histidines in a distorted tetrahedral geometry, the purple CuA site consists of a mixed-valent [$Cu^{1.5}$−$Cu^{1.5}$] center with one histidine bound to each copper and two cysteines forming bis(μ-dithiolato) bridges between two closely lying metal atoms (*8*, *9*). An understanding of the conformational properties and biochemical implications of the binuclear copper center has attracted extensive interest in recent years.

The complexity of the structure and spectroscopy of the intact cytochrome *c* oxidase had earlier made the study of the CuA site difficult, since the spectroscopic features of this site were almost completely masked by those of the heme centers of the enzyme (*12*). Soluble fragments of subunit II containing the CuA domain (Figure 1) have been recently prepared from bacterial CcO of various sources [e.g., *Paracoccus denitrificans* (*13*), *Bacillus subtilis* (*14*, *15*), *Thermus thermophilus* (*16*), and *Paracoccus versutus* (*17*)]. Modified CuA containing soluble domains of ubiquinol oxidase from *Escherichia coli* (CyoA) (*18*) as well as the engineered dicopper site in "blue copper" proteins amicyanine (*15*, *16*) and azurin (*19*, *20*), have also been made. Extensive biochemical, spectroscopic, and kinetic studies on

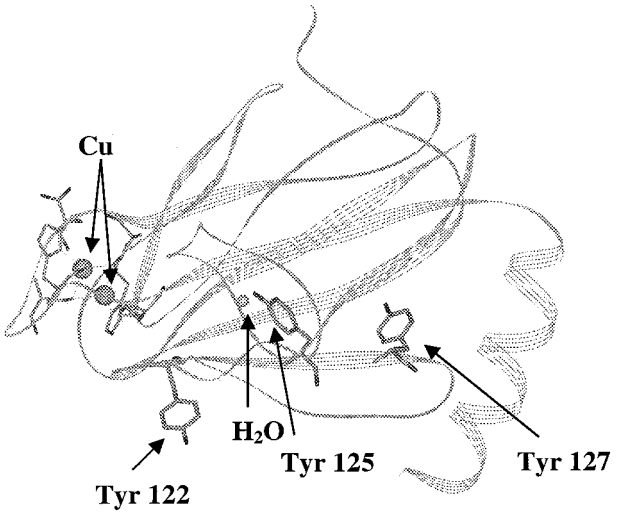

FIGURE 1: Schematic structure of the soluble domain of subunit II of cytochrome oxidase from *P. denitrificans* with the transmembrane part deleted and the tyrosines, the copper site, and the water molecule inside the β-barrel core shown. The structure was taken from the RCSB Protein Data Bank (PDB code 1AR1).

† This work was supported by the Tata Institute of Fundamental Research.

* Address correspondence to this author. Fax: +91 22 215 2110. Tel: +91 22 215 2971 ext 2605. E-mail: shyamal@tifr.res.in.

‡ Tata Institute of Fundamental Research.

§ European Molecular Biology Laboratory.

10.1021/bi002212e CCC: $20.00
Published on Web 04/28/2001

the water-soluble CuA-containing fragment of CcO as well as on the engineered CuA centers have recently been carried out to investigate the structure−function relationship of this unique metal center (*12*, *17*, *21*−*24*). These studies helped to assign the visible absorption and CD bands of the CuA site, which originate predominantly due to LMCT transitions from cysteine to copper. pH-dependent studies further showed that increase in pH causes drastic change in the absorption spectrum of the binuclear copper site (*12*, *13*). Recent NMR studies on subunit II of cytochrome *c* oxidase of *P. versetus* indicated that one of the coordinated histidines (H224) possibly moves away at high pH, forming a "valence-trapped" system (*17*). Mutagenic replacement of the solvent-exposed histidine H224 (H224N) has been shown to result in a species that is spectrocopically similar to the high-pH form of the protein (*12*, *13*). Such change in the coordination geometry would require significant change in the conformation of the protein in the vicinity of the metal centers. The structure of the protein shown in Figure 1 indicates the presence of a large number of β-sheets forming a β-barrel motif. Such extensive β-barrel cupredoxin topology (*25*, *26*) of the CuA site may have a significant effect in imparting specific coordination geometry of the dicopper center, and slight changes in this β-barrel structure may alter the conformational properties of the metal site. A pK_a of 8.2 was associated with the pH-induced change in the absorption spectra, indicating possible involvement of a tyrosine residue in this process (*12*, *13*), although any structural relevance of this pK_a is yet to be established.

The present report describes studies on conformational properties of the "low-pH" and the "high-pH" forms of the soluble CuA of *P. denitrificans*. pH-dependent circular dichroism and stopped-flow pH-jump studies have been carried out to understand the nature of the conformation change of the protein associated with the change in pH. Thermal unfolding of the metal active site has also been studied at different pHs. Thermodynamic stabilities of the copper site as well as of the overall structure of the protein have been investigated using urea-induced denaturation of the protein at different pHs. The effect of pH on the overall stability of the protein in different oxidation states of the metal ions has also been investigated. The results have been discussed in the light of understanding the conformational properties of the binuclear CuA site.

MATERIALS AND METHODS

Protein Purification. Expression and purification of the soluble fragment of subunit II (PdII) of cytochrome *c* oxidase of *P. denitrificans* were performed (*13*) according to Lappalainen et al. The SDS−PAGE of the purified PdII showed a single band corresponding to >95% purity. The pure protein was characterized by the ratio of absorbances at 280 and 480 nm as 11.2 (A_{280}/A_{480} = 11.2) at pH 7. Protein concentration was measured using an extinction coefficient (ϵ_{280}) of 48.7 mM^{-1} cm^{-1} at 280 nm (*13*). All chemicals used were of the highest analytical grade.

Spectroscopic Methods. Optical spectra were recorded on a Shimatzu UV2100 spectrophotometer attached to an IBM PC-486 and equipped with a thermostated cell holder for variable temperature experiments. Optical absorption was measured between 250 and 900 nm. All the optical spectral studies were carried out with protein concentrations in the range of 20−60 μM.

Circular dichrosim studies were carried out using a Jasco J-600 spectropolarimeter equipped with a thermostated cell holder for variable temperature experiments. Visible and near-UV CD experiments were carried out using protein concentrations of ∼15−30 μM, and the path length of the cuvette was 10 mm. Far-UV CD studies were carried out using a 1 mm cuvette with ∼10 μM protein concentration. Far-UV CD spectra were measured over the 200−260 nm range, and each spectrum was taken by averaging over 20 scans. Near-UV and visible CD spectra were collected in the spectral ranges of 250−300 and 300−700 nm, respectively. A good signal-to-noise ratio in the CD spectra in this spectral range was obtained on data averaging over three to four scans.

Stopped-flow kinetic experiments were carried out using a Hi-Tech SF61MX stopped-flow spectrometer. The sampling unit was mounted inside a thermostated bath compartment, and the temperature of the compartment was maintained (within ±1 °C) using a circulating water bath. The protein was dissolved in 20 mM bistrispropane hydrochloride buffer. The pH jump was achieved in the stopped-flow mixing chamber by mixing the protein solution (at initial pH = pH_i) to an equal volume of the buffer at different pHs to give the final pH (pH_f) of the solution. The pH of the final mixture (pH_f) was precalibrated by externally mixing the same proportions of the buffers.

pH Titration. UV−visible absorption, visible CD, and near-UV CD were used to monitor the pH-induced conformational changes of PdII. The pH was varied from 6 to 10 using 20 mM bistrispropane hydrochloride buffer at room temperature (23 °C). The pH was varied in both directions to check the reversibility of the conformational transition.

Thermal Unfolding. Visible, near-UV, and far-UV CD as well as UV−visible absorption spectra were used to monitor the thermal unfolding of PdII at pH 6.0 and at pH 10.5 using 50 mM phosphate buffer and 50 mM borate hydrochloride buffer, respectively. The composition of the buffer did not have any effect on the spectral properties of the protein. The temperature was varied from 15 to 60 °C in steps of 5 °C with an equilibration time of 2 min at each temperature. The reversibility of the conformational change was checked by monitoring the absorption spectra at room temperature upon cooling immediately after the end of the experiment. In all the cases the temperature course was precalibrated by positioning a thermocouple in the cuvette. Care was taken to maintain constant ionic strength of the solutions at different pHs.

Urea-Induced Unfolding. UV−visible absorption and far-UV CD were used to monitor the urea-induced unfolding of the native, i.e., mixed-valence ($Cu^{1.5}$−$Cu^{1.5}$), and the reduced ($Cu^{1.0}$−$Cu^{1.0}$) PdII at pH 6.0 and at pH 10.0. Aliquots of the protein solution were equilibrated with various urea concentrations ranging from 0 to ∼10 M for 60 min at room temperature, and spectra were taken. Reversibility of the unfolding transition was checked by diluting the protein sample at high urea concentration into the buffer solution and recording its ellipticity at 222 nm. The urea concentration in the stock solutions was checked using a refractometer according to the reported method (*27*).

Data Analysis. In both the thermal unfolding and urea-induced unfolding experiments, data were analyzed in terms of a two-state equilibrium model (*27*, *28*):

$$\text{native (N)} \rightleftarrows \text{unfolded (U)} \quad (1)$$

The apparent equilibrium constant of unfolding (K_{eq}) and free energy change (ΔG) were estimated in the transition region by the relations:

$$K_{eq} = \frac{y_n - y}{y - y_d} \quad (2)$$

$$\Delta G = -RT \ln(K_{eq}) \quad (3)$$

where y is the spectral property (absorbance or ellipticity) observed at a given temperature or urea concentration. y_n and y_d are the spectral properties characteristic of the native (N) and the unfolded (U) protein, respectively. y_n and y_d were determined from the extrapolation of linearly fitted pre- and post-transitional baselines of the transition curve against the temperature or urea concentration (*27*, *28*).

The equilibrium constant for thermal unfolding ($K_{T,eq}$) at temperature T is related to the corresponding free energy of unfolding (ΔG_T):

$$\Delta G_T = -RT \ln(K_{T,eq}) = \Delta H_T - T\Delta S_T \quad (4)$$

where ΔH_T and ΔS_T are the enthalpy and entropy changes at temperature T for this process. At the midpoint of the transition, i.e., $T = T_m$, $\Delta G_{Tm} = 0$. The van't Hoff plot of $\ln(K_{T,eq})$ against $1/T$ was linearly fitted to

$$\ln(K_{T,eq}) = \frac{\Delta S_{Tm}}{R} - \frac{\Delta H_{Tm}}{R}\left(\frac{1}{T}\right) \quad (5)$$

where ΔH_{Tm} and ΔS_{Tm} are respectively the standard enthalpy and standard entropy changes at the midpoint temperature (T_m). The enthalpy and entropy changes associated with unfolding of the protein depend on temperature. The experimental $\ln(K_{T,eq})$ (eq 4) was corrected for temperature dependence in ΔH_{Tm} and ΔS_{Tm} using the reported method by considering the contributions of the specific heat changes in the temperature range studied (*29*).

The plots of ΔG against urea concentration were analyzed by linear least-squares analysis, according to the two-state model, by using the equation:

$$\Delta G = \Delta G(H_2O) + m[\text{urea}] \quad (6)$$

where m is the dependency of the ΔG on urea concentration, which is a measure of cooperativity of unfolding (*28*), and $\Delta G(H_2O)$ is the free energy change in the absence of denaturant, which is equivalent to conformational stability of the protein. The midpoint of denaturation, C_m, can be determined from eq 6 and corresponds to the urea concentration where $\Delta G = 0$. The urea-induced unfolding curve was also fitted to a nonlinear least-squares analysis using the equation

$$y = y_n + y_d \frac{\exp[-\Delta G/RT]}{1 + \exp[-\Delta G/RT]} \quad (7)$$

The values of ΔG are given by eq 3.

RESULTS

pH- and Temperature-Induced Conformation Change. The UV−visible absorption and visible CD spectra of the CuA site (PdII) show significant changes with pH. Figure 2a (upper panel) shows the UV−visible spectra of PdII at pH 6 and at pH 10, which match with earlier reports (*12*, *13*). Plots of the apparent extinction coefficient (calculated from the absorbance of the protein) at the absorption maxima against pH, shown in the lower panel of Figure 2a, gave an inflection point at pH ~8.2 which agrees with earlier report (*13*). The solid lines through the data plotted in the lower panel of Figure 2a represent sigmoidal fits. Lappalainen et al. (*13*) pointed out possible involvement of a tyrosine residue lying close to the copper center, in the observed pH-dependent spectral change of the protein. They also proposed that at high pH the deprotonated tyrosine might coordinate with a copper through oxygen ligation. Site-directed mutagenesis (*12*, *13*) and NMR (*17*) studies indicated breaking of the coordinate bond between a copper and H224 at high pH.

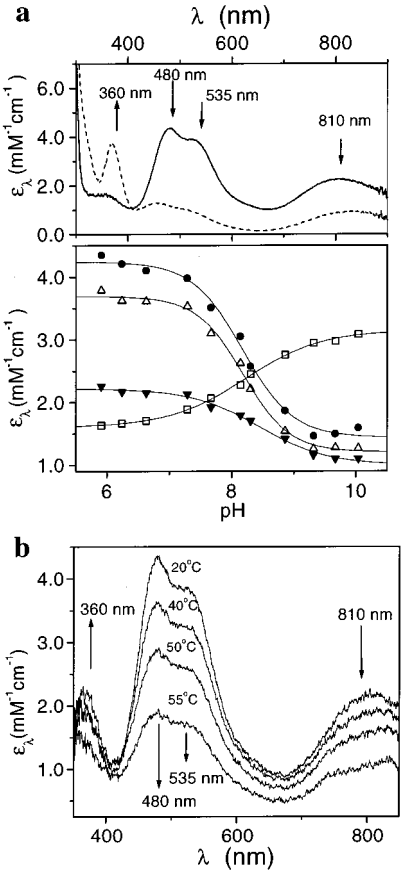

FIGURE 2: (a) The upper panel shows UV−visible absorption spectra of PdII [extinction coefficients (ϵ_λ) are plotted against wavelength, λ] at pH 6.0 (solid lines) and at pH 10.0 (dashed lines). The variation of extinction coefficients with pH was monitored at the wavelengths shown by vertical arrows. The variation of absorbance with pH is shown in the lower panel: □, 360 nm; ●, 480 nm; △, 535 nm; ▼, 810 nm. Solid lines represent sigmoidal fits to the data. (b) Variation of the UV−visible absorption spectra of PdII with increasing temperature at pH 7.0 from 20 to 55 °C. Vertical arrows show the direction of change in the absorption with increase in temperature at different wavelengths. The spectra disappear at temperatures above 65 °C, indicating depletion of the metal center.

Figure 2b shows that an increase in temperature of a solution of PdII at ambient pH (pH 7) from 20 to ~55 °C was associated with a gradual decrease in the absorbance of the 480, 535, and 810 nm absorption bands with a subsequent

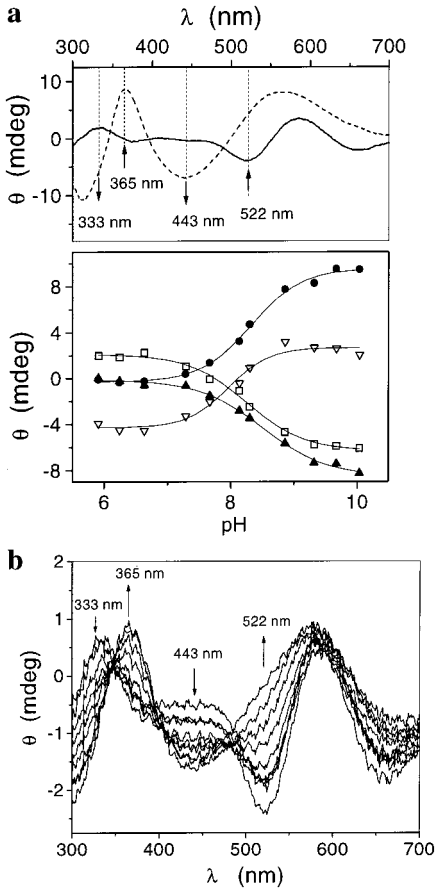

FIGURE 3: (a) The upper panel shows visible CD spectra of PdII (~30 μM) at pH 6.0 (solid lines) and at pH 10.0 (dashed lines). The variation of CD with pH was monitored at the wavelengths shown by vertical arrows and dotted lines. The plot of variation of absorbance against pH is shown in the lower panel: □, 333 nm; ●, 365 nm; ▲, 443 nm; ▽, 522 nm. Solid lines represent sigmoidal fits to the data. (b) Variation of CD spectra of PdII (~5 μM) with temperature at pH 7.0 from 25 to ~50 °C. Vertical arrows show the direction of change in the CD with increase in temperature at different wavelengths.

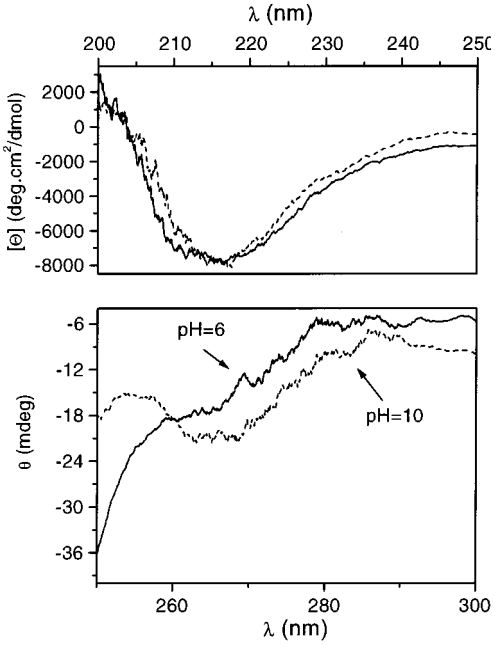

FIGURE 4: The upper panel shows far-UV CD spectra of PdII (mean residue ellipticity [Θ] is plotted against wavelength) at pH 6.0 (solid lines) and at pH 10.0 (dotted lines). The lower panel shows the near-UV CD spectra of PdII (~20 μM) at pH 6.0 (solid lines) and at pH 10.0 (dotted lines).

increase in the 360 nm band. This result is qualitatively very similar to the effect of an increase in pH of the protein solution shown in Figure 2a.

The CD spectra of PdII in the visible region (Figure 3a) showed an increase in ellipticity of the 365 and 522 nm bands at the expense of the 333 and 443 nm bands with an increase in pH from 6.0 to 10.0. The plots of the ellipticity of CD bands against pH shown in the lower panel of Figure 3a follow sigmoidal behavior (solid lines show sigmoidal fits to the data) similar to that observed in the case of the pH dependence of the absorption maxima (lower panel of Figure 2a). These results thus show that the pH dependence of the protein was associated with a pK_a of ~8.2 (lower panels of Figures 2a and 3a).

The CD spectral change of PdII (at pH ~7) on increase in temperature from 25 to 55 °C shown in Figure 3b, was analogous to that observed on increasing the pH of the protein solution (Figure 3a). These spectral changes of PdII thus arise due to conversion from a low-pH to a high-pH species possibly caused by breaking of the H-bonding network. However, at temperatures above ~65 °C, denaturation of the CuA site takes place, which is characterized by a fast irreversible decrease of all absorption and CD bands in the visible region.

Reversible conversion from the low-pH to the high-pH species on increase in temperature was observed in the pH range ~7.0−8.0 (Figures 2b and 3b). However, no such thermal interconversion was observed at pH below 6.5 when only the low-pH species was present and at pH above ~9 when only the high-pH species was present. Increase in temperature of the protein solution at pH 6 showed thermal unfolding of the low-pH species, and that at pH 10 showed thermal unfolding of the high-pH species with no significant detectable interconversion to the other form of the protein.

The CD spectrum of the protein in the far-UV region remains almost independent of pH (upper panel of Figure 4) or temperature up to 55 °C (data not shown), indicating that the overall secondary structure of the protein remains almost unchanged in this pH range in the temperature range from ambient to 55 °C. The magnitudes of the mean residue ellipticity ([Θ] in deg·cm^2/dmol) for PdII in the far-UV region were calculated to determine the helical content of the protein. Analysis of the CD spectrum of the protein in the far-UV region by the neural network method using the CDNN program (*30*) showed that there is ~14% helicity in the protein, and no change in the helicity was observed on increase in pH from pH 6 to pH 10.

However, the CD at 280 nm region (near-UV CD), which is characteristic of the tertiary structure of the protein, undergoes a definite change with pH (lower panel in Figure 4) as well as with temperature (data not shown). The effects of increase in pH and increase in temperature on the CD spectra of the protein in this region were similar. These results show that although the overall secondary structure of the protein remains almost unchanged, a local tertiary structure of the protein is possibly affected due to breaking of the hydrogen-bonding network caused by an increase in pH or increase in temperature of the protein solution.

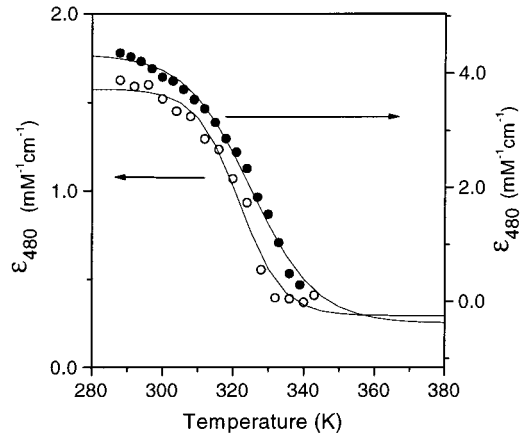

FIGURE 5: Variation of the apparent extinction coefficent at 480 nm (ϵ_{480}) of PdII at pH 6.0 (●) and at pH 10.0 (○) with temperature. Solid lines represent sigmoidal fits to the data.

The thermal stability of the tertiary structure of the protein would be affected due to breaking of the hydrogen-bonding network in the protein. Equilibrium thermal unfolding of the low-pH form and the high-pH form would help to understand the effect of hydrogen bonding on the stability of the protein in these two conformational states. Figure 5 shows representative plots of apparent extinction coefficients at 480 nm (ϵ_{480}) against temperature at the two extreme pH values. Analogous plots were also obtained from the variation in CD in the visible region (data not shown). The midpoint of the unfolding transition (T_m), determined from sigmoidal fits to the experimental absorbance or CD with temperature, was found to be 60 ± 3 °C at pH 6 and 48 ± 3 °C at pH 10, indicating that the thermal stability of the metal site is decreased at higher pH (Figure 5). It is, however, important to note that the thermal unfolding curves were reversible up to 65 °C as characterized by absence of hysteresis, and irreversible denaturation becomes predominant, leading to depletion of metal ions from the protein above this temperature. The values of ΔH_{Tm} for melting of the binuclear site were found to be 340 ± 2 and 124 ± 2 kJ/mol, respectively, at pH 6.0 and 10.0, while the corresponding values of ΔS_{Tm} were 1000 ± 50 and 386 ± 50 J mol^{-1} K^{-1}, respectively.

Isothermal Equilibrium Unfolding by Denaturant. The stability of the overall structure of the protein can be probed by monitoring equilibrium unfolding using denaturants such as urea or guanidinium chloride (*27*, *28*). The midpoint (C_m) of the unfolding curve is a measure of the stability of the protein toward unfolding. Figure 6 shows a plot of the apparent extinction coefficients at 480 nm (ϵ_{480}) and CD (ellipticity, θ, in millidegrees) at 522 and 443 nm of PdII at pH 6 and at pH 10, respectively, against increasing concentrations of urea. The solid lines in Figure 6 represent sigmoidal fits to the experimental data. Variations of the absorbance at 480 nm and CD at 522 nm and at 443 nm are measures of unfolding of the binuclear copper site. The results in Figure 6 show that the C_m for unfolding of the metal site is 6.0 ± 0.2 M at pH 6, which is decreased to 2.5 ± 0.2 M at pH 10, indicating that the stability of the tertiary structure around the metal site is drastically decreased at high pH. The unfolding transition probed from the spectral variations in the visible region corresponds to changes in the tertiary structure around the binuclear copper center, and the final unfolded form is characterized by the complete

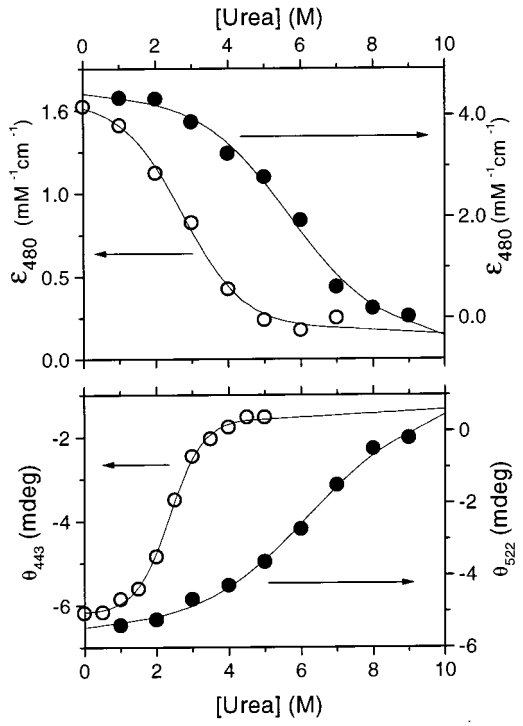

FIGURE 6: The upper panel shows variation of the apparent extinction coefficient at 480 nm (ϵ_{480}) of PdII at pH 6.0 (●) and at pH 10.0 (○) with urea. The lower panel shows variation of the ellipticity of PdII (~25 μM) at 522 nm (θ_{522}) at pH 6.0 (●) and at 443 nm (θ_{443}) at pH 10.0 (○) with urea. Solid lines represent sigmoidal fits to the data.

absence of the spectra, indicating depletion of the metal ion from the protein.

To understand the conformational stability of the overall secondary structure of the protein, equilibrium unfolding of the secondary structure was studied by monitoring the far-UV CD (CD at 222 nm) of the protein in the presence of urea. Figure 7 shows a plot of the CD at 222 nm of PdII (~10 μM) with increasing concentrations of urea at pH 6.0 and at pH 10. The solid lines in Figure 7 represent fits to the experimental data using eq 7. The unfolding free energies were calculated using eq 3 from the experimental results at different urea concentrations (plots shown in Figure 8), and variation of the free energy with denaturant concentration was fitted using eq 6. A linear dependency of the unfolding free energy on the urea concentration was found, as illustrated by solid lines in Figure 8. The results show that the free energy of unfolding of the native protein in water [$\Delta G(H_2O)$ = 14 ± 3 kJ/mol] at pH 6.0 is higher than that at pH 10.0 [$\Delta G(H_2O)$ = 7 ± 3 kJ/mol], indicating that the conformational stability of the low-pH species is higher than that of high-pH species. The value of C_m for the low-pH form (3.4 ± 0.8 M) is also much larger than that for the high-pH form (1.2 ± 0.8 M). The sharp decrease in the midpoint concentration (C_m) of the protein in the high-pH form suggests lower overall stability of the secondary structure of the protein at high pH.

The stability of the redox protein is often dependent on the oxidation state of the metal ion (*29*, *31*, *32*). The copper ion can have variable oxidation states and coordination geometries which can affect the local conformation of the metal active site within a protein environment. Earlier studies (*29*) on subunit II of CcO of thermostable bacteria (*T.*

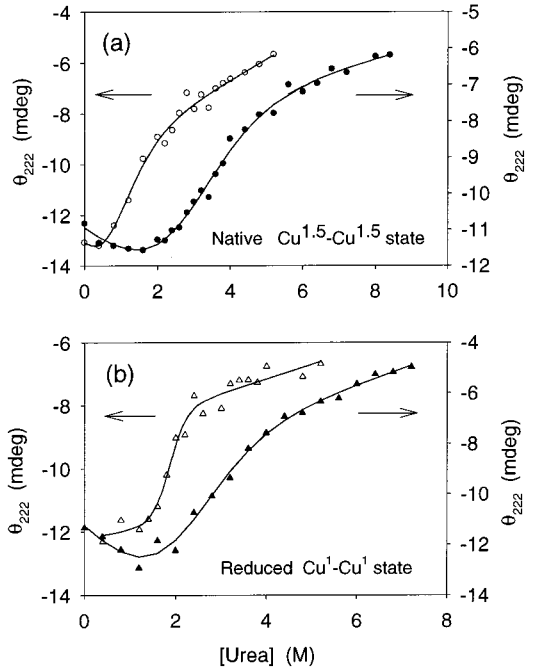

FIGURE 7: (a) Variation of the ellipticity at 222 nm (θ_{222}) of mixed-valence PdII (~10 μM) at pH 6.0 (●) and at pH 10.0 (○) with urea. (b) Variation of the ellipticity at 222 nm (θ_{222}) of reduced PdII (~10 μM) at pH 6.0 (▲) and at pH 10.0 (△) with urea. Solid lines through the data represent the best fit to eq 7.

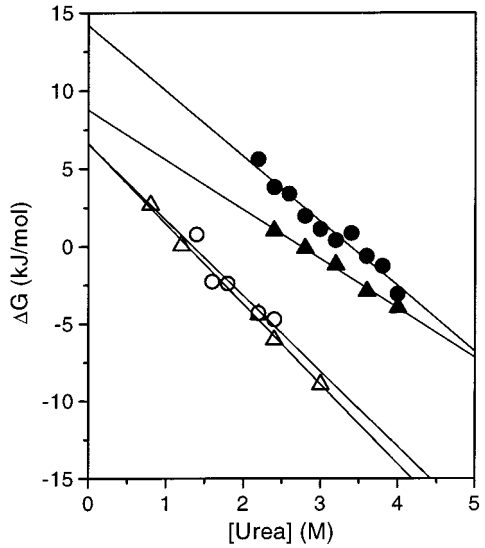

FIGURE 8: Plot of the linear relation between free energy ΔG and urea concentration for unfolding the PdII (eq 6): mixed-valence state ($Cu^{1.5}$−$Cu^{1.5}$) at pH 6.0 (●) and at pH 10.0 (○); reduced state ($Cu^{1.0}$−$Cu^{1.0}$) at pH 6.0 (▲) and at pH 10.0 (△). Extrapolation to 0 M urea gives the free energy [$\Delta G(H_2O)$] for the protein unfolding in water. Solid lines through the data represent the best fit to eq 6.

thermophilus) showed that the conformational stability of the protein at the native mixed-valence state is more than that of the fully reduced form at ambient pH. To investigate the effect of the oxidation state of the metal ions on the overall stability of PdII, urea-induced unfolding of the secondary structure of the protein was carried out on the reduced protein. The unfolding free energy for the reduced PdII was also found to show linear dependency with denaturant as expected from eq 6. The thermodynamic parameters determined from the unfolding study are tabulated in Table 1. Table 1 shows that the $\Delta G(H_2O)$ for PdII at pH 6.0 is higher (14 ± 3 kJ/mol) for the mixed-valence state than that for reduced state (9 ± 3 kJ/mol). This trend agrees with that observed in the case of subunit II of the thermostable species at neutral pH as well as with most other electron-transfer copper proteins (*29*, *31*). The value of $\Delta G(H_2O)$, however, is almost independent of the oxidation state of the metal ion at pH 10.0 [$\Delta G(H_2O)$ 7 ± 3 kJ/mol], indicating that there is no significance difference in conformational stability of the mixed-valence and the reduced species of the high-pH form. The midpoint concentrations (C_m) for the reduced protein were found to be 2.7 ± 0.8 and 1.3 ± 0.8 M at pH 6.0 and at pH 10.0, respectively. This indicated that the reduced protein unfolds at a lower urea concentration than that required for the native (mixed-valence) species in the low-pH form, while the high-pH form of the protein shows unfolding at almost the same urea concentration in both the native and reduced oxidation states. Superoxidation to the fully oxidized form [Cu^{2+}−Cu^{2+}] of the protein cannot be stabilized in the present case (*12*).

Stopped-Flow Kinetics. The kinetics of conversion from the low-pH form to the high-pH form was studied by the stopped-flow pH-jump method. The time dependence of the absorbance at 360, 480, and 810 nm on the change in the pH of the solution was monitored. The time evolution of the observable (y) in a stopped-flow kinetic trace was fitted to a single-exponential model

$$y = A \exp(-t \times k_{app}) + B \qquad (8)$$

where t is time, k_{app} is the apparent rate constant, and A and B are constants.

Figure 9 shows a typical stopped-flow transient kinetics trace (middle panel of Figure 9) of the conformational change of the binuclear site obtained by a pH jump from pH 6.5 (pH_i) to pH 9.5 (pH_f). The change in the apparent extinction coefficient in each of these wavelengths was best fitted to a single-exponential function (eq 8), and the apparent rate constant (k_{app}) was calculated at each pH. The top panel in Figure 9 shows typical residuals distribution in the single-exponential analysis to the experimental data indicating goodness of the fit. Similar experiments were carried out by varying the initial pH (pH_i) and the final pH (pH_f) in the stopped-flow pH-jump kinetics of the protein solution. The time dependence of absorbance was found to follow a single-exponential function (eq 8), and the values of k_{app} were evaluated at each pH. The magnitude of the apparent rate constant (k_{app}) was found to be independent of the initial pH (pH_i) in the pH-jump experiment. This indicated that the change in pH of the solution on mixing of two buffers takes place within the mixing time of the instrument, and the rate of the reaction depends only on the final pH (pH_f). The lower panel of Figure 9 shows that the experimental k_{app} decreases with increase in final pH. The inset in the lower panel of Figure 9 shows a plot of k_{app} against [H^+] concentration, and the solid line shows a linear fit to the data.

DISCUSSION

The CuA site of PdII (Figure 1) contains a dicopper center with two cysteines (C216, C220) forming dithiolate bridges between the copper centers (*8*, *9*). A histidine and a methionine (H181, M227) are bound to one copper while the other copper is coordinated to another histidine and a

Table 1: Analysis of Urea Denaturation of the CuA Domain of PdII and of *T. thermophilus* at the Native Mixed Valence State and at the Reduced State of the Metal Center[a]

	$\Delta G(H_2O)$ native (kJ/mol)	C_m native (M)	m native (kJ/mol)	$\Delta G(H_2O)$ reduced (kJ/mol)	C_m reduced (M)	m reduced (kJ/mol)
PdII at pH 6.0	14 ± 3	3.4 ± 0.8	4 ± 1	9 ± 3	2.7 ± 0.8	3 ± 1
PdII at pH 10.0	7 ± 3	1.2 ± 0.8	5 ± 1	7 ± 3	1.3 ± 0.8	5 ± 1
T. thermophilus[b] CuA domain at pH 7.0	85			65		

[a] m and $\Delta G(H_2O)$ were estimated from plots of ΔG versus urea concentration fitted to eq 6 (Figure 8). C_m is the concentration of urea corresponding to the midpoint of denaturation where $\Delta G = 0$. [b] Taken from ref *5*.

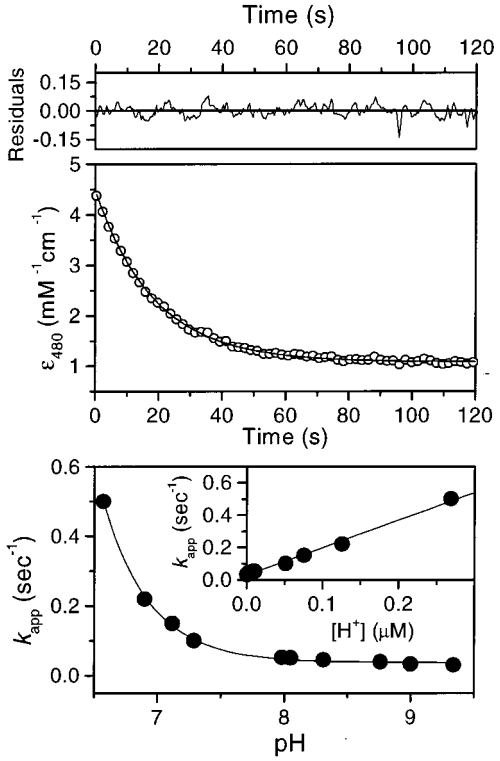

FIGURE 9: Time-dependent variation of the apparent extinction coefficient at 480 nm (ϵ_{480}) of PdII obtained in the stopped-flow pH jump from pH 6.5 to pH 9.5 (shown in the middle panel). Residual distribution is shown in the top panel. The lower panel shows variation of the k_{app} with pH (●). The solid line represents the fit to eq 12 ([H$^+$] in eq 12 is written as 10^{-pH}). The inset in the lower panel shows a plot of k_{app} against [H$^+$] concentration, and a linear fit to the data using eq 12 is shown by solid line.

glutamic acid (H224, E218) (*8*, *9*). The native form of the protein has a small (2.48 Å) Cu−Cu distance, leading to significant charge delocalization resulting in a mixed-valent [$Cu^{1.5}$−$Cu^{1.5}$] state (*8*, *33*). The geometry of the ligands coordinated to the metal center are not symmetric (*8*, *33*). A detailed analysis of optical absorption, MCD, and CD spectra of the binuclear copper site (CuA) of nitrous oxide reductase (N_2OR) from *P. stutzeri* (*22*), cytochrome *c* oxidase from *P. denitrificans* (*12*, *13*, *22*), genetically engineered subunit II of *E. coli* ubiquinol oxidase (*22*), CuA azurin (*19*, *34*), and the CuA domain from *T. thermophilus* (*16*) shows that there is a variation in the spectral properties of the CuA center from different sources. Investigation of the high-resolution structure of the CuA site of *P. denitrificans* (*8*), CuA azurin (*33*), *E. coli* ubiquinol oxidase purple CyoA (*6*), and the CuA domain of *T. thermophilus* (*7*) revealed that both the angular position of the nitrogen atoms of the coordinated histidines with respect to the Cu_2S_2(Cys) core plane and the axial ligands interacting with the copper center are important in the fine-tuning of the electronic structure and functional properties of the CuA center.

Two Conformational States: Low-pH and High-pH Forms Are in Equilibrium. The visible absorption bands of PdII (Figure 2a) have been assigned to be predominantly due to charge-transfer transitions between the copper and cysteine and histidine residues (*22*) in the mixed-valence [$Cu^{1.5}$−$Cu^{1.5}$] species (*13*). Thus the reduced copper site does not show these absorption bands. The pH dependence of the absorption bands shows sigmoidal behavior (lower panel of Figure 2a) with pH, which supports the existence of a single-step equilibrium between a low-pH (P_AH) and a high-pH (P_B) form:

$$\text{low-pH form } (P_AH) \rightleftarrows \text{high-pH form } (P_B) + H^+ \quad (9)$$

The pK_a for this transition was found to be 8.2, indicating that the low-pH form would predominate at ambient pH and the high-pH form would be predominant at pH above ~8. Any ligand exchange process such as coordination of a tyrosine residue (*13*) at high pH would have shown significant shift in the band positions with increase in pH, which was not observed in the present case. Small changes in the absorption peak positions along with changes in the intensities of the bands in the present case might thus arise due to small distortions in the coordination site of the dicopper center.

Analogous pH dependence in the circular dichroism spectra of the protein (Figure 3a) in the visible region supports the possibility of a change in the conformation of the binuclear site with increase in pH. The results thus suggest that deprotonation of an amino acid with p$K_a = 8.2$ is possibly involved in the conformational transition at the metal site. The far-UV CD spectral studies (upper panel of Figure 4) indicated that the pH-induced conformational transition did not affect the overall secondary structure of the protein. The tertiary structure of the protein determined from the near-UV CD (lower panel of Figure 4), however was drastically changed on transition from the low-pH to the high-pH forms. These results suggest that the pH-induced equilibrium conversion of the low-pH form to the high-pH form is associated with a conformational change possibly localized near the binuclear copper site of the protein. Reversibility of the equilibrium between these two forms was further verified by thermal interconversion from the low-pH to the high-pH forms of the protein solution at ambient pH. The results suggest that the equilibrium (eq 9) between the low-pH and high-pH forms possibly shifts toward the right-hand side on increase in temperature, which agrees with the fact that it is an endothermic process.

Thermal Stability of the Low- and High-pH Forms. Considering the equilibrium between the two conformations ($pK_a = 8.2$), the concentration of the low-pH form would be >99% at pH 6.0. Thus, the spectral changes associated with increase in temperature of the protein solution at pH 6.0 would be associated with thermal unfolding of the low-pH form of the protein. Similarly, thermal unfolding of the high-pH form takes place with increase in temperature at pH 10.5. Analysis of the thermal unfolding curves (Figure 5) showed that the midpoint temperature (T_m) and enthalpy (ΔH_{Tm}) of thermal unfolding of the low-pH form were higher compared to the high-pH form, indicating higher thermal stability of the binuclear site in the low-pH form. This suggests that the tertiary structure around the metal ions in the low-pH form is stabilized by a hydrogen-bonding network which is broken on increase in pH to produce the less stable conformation in the high-pH form. The breaking of the hydrogen-bonding network could lead to a change in the local tertiary structure, which in turn would affect the conformation of the binuclear copper site. The soluble fragment of subunit II of CcO from *T. thermophilus* has earlier been shown to be highly stable with a T_m of >100 °C for the oxidized and 83 °C for the reduced protein in absence of any denaturant, which were shown to decrease in the presence of Gdn·HCl. The standard enthalpy change (ΔH_{Tm}) for thermal unfolding of the thermostable protein is also very high, which decreases in the presence of denaturant. The value of ΔH_{Tm} for the thermostable protein in the presence of 5.5 M Gdn·HCl was comparable to that observed in the present case without denaturant. This is in agreement with the fact that the thermodynamic stability of the *Paracoccus* protein (PdII) is much lower compared to the thermostable one.

Conformational Stability of the Binuclear Site and Stability of the Overall Protein Structure in the Low-pH and the High-pH Forms. The thermodynamics of unfolding of the protein has been studied using urea as the denaturant. Gdn·HCl binds to the surface carboxylate residues of the protein leading to coagulation; hence, it was not suitable for the study of denaturation of PdII.

The visible and near-UV CD spectra as well as the visible absorption spectra of the protein showed a significant change in intensities of all bands due to unfolding of the tertiary structure around the binuclear copper center (CuA) of the protein in the presence of urea. The low C_m of the high-pH form may indicate less rigidity of the tertiary structure of the binuclear site at high pH (Figure 6). The results thus indicate that the coordination geometry of the metal ions in the low-pH form is possibly more stable compared to the high-pH form. It is to be noted that urea-induced unfolding of the copper site leads to depletion of the metal ion from the protein, resulting in formation of apo-PdII. Moreover, since the apoprotein of PdII will have free cysteine residues just four amino acids apart (C216 and C220), they can form disulfide bonds with each other. This may prevent reversible incorporation of copper at the binuclear site, and one needs to add excess DTT and copper ion in order to reconstitute the metal site in the protein. Thus, unfolding of the binuclear site by urea is apparently an irreversible process.

Unfolding of the secondary structure of PdII monitored by the change in far-UV CD at 222 nm gives an estimate of the overall conformational stability (Figure 7) of the protein. This is a two-state reversible process. The denaturation curves were analyzed using eq 6 to determine the values of free energy of unfolding [$\Delta G(H_2O)$] (Table 1). Interesting redox state dependent stability of the secondary structure of the protein was observed analogous to that reported in the case of the themostable protein (Table 1). The low-pH form of the protein was found to be more stable in the mixed-valence [$Cu^{1.5}-Cu^{1.5}$] oxidation state compared to the corresponding reduced [$Cu^{1.0}-Cu^{1.0}$] protein. The thermodynamic stability of the secondary structure of the high-pH form was, however, almost independent of the oxidation states of the metal ions. Moreover, the overall stability of the high-pH form was lower than that of the low-pH form of PdII both in the oxidized and in the reduced states of the metal center. The prosthetic group in many proteins has been shown to stabilize the native conformation of the metalloprotein (*31*, *35*), and if the protein is redox active, the degree of stabilization often depends on the oxidation state of the metal ion. Reduced cytochrome *c* has been shown to have a larger free energy of unfolding than the oxidized protein (*23*), while the blue copper protein, azurin (*31*, *35*), and the binuclear copper site (CuA) of *T. thermophilus* cytochrome oxidase (*29*) have a larger free energy of unfolding in the oxidized native state of the copper atom. The results of the present study showed that the PdII is also more stable in the oxidized native state of the metal ions compared to the reduced species.

Mechanism of pH-Induced Conformational Transition. The conversion from the low-pH (P_AH) to the high-pH (P_B) form of PdII induced by an increase in pH involves two main steps, one involving deprotonation of an amino acid leading to the formation of the deprotonated species (P_A^-) which may still maintain the conformation of the low-pH form. This step is then followed by conformational rearrangement in which the tertiary structure around the metal site is changed, leading to formation of the high-pH form. The following two reaction schemes (eqs 10a,b and 13a,b) are possible under such circumstances:

$$\text{step 1:}\quad \text{low-pH form } (P_AH) \underset{k_2}{\overset{k_1}{\rightleftharpoons}} \text{low-pH form } (P_A^-) + H^+ \quad (10a)$$

$$\text{step 2:}\quad \text{low-pH form } (P_A^-) \overset{K_{iso}}{\rightleftharpoons} \text{high-pH form } (P_B) \quad (10b)$$

where step 1 is the rate-determining step which is followed by fast conformational equilibrium (K_{iso}). The time evolution of the concentration of the low-pH form (P_AH) in eq 10 would be given as

$$[P_AH] = [P_AH]_f - ([P_AH]_f - [P_AH]_i) \times \exp\left[-\left(k_1 + \frac{k_2[H^+]_f}{1 + K_{iso}}\right)t\right] \quad (11)$$

where $[P_AH]_i$ and $[P_AH]_f$ are the concentrations of the low-pH form at initial (pH_i) and final pH (pH_f). The apparent rate constant in eq 10 would thus be

$$k_{app} = \left(k_1 + \frac{k_2[H^+]_f}{1 + K_{iso}}\right) \quad (12)$$

$$\text{step 1: low-pH form } (P_AH) \overset{K_a}{\rightleftharpoons} \text{low-pH form } (P_A^-) + H^+ \quad (13a)$$

$$\text{step 2: low-pH form } (P_A^-) \underset{k_4}{\overset{k_3}{\rightleftharpoons}} \text{high-pH form } (P_B) \quad (13b)$$

where step 2 is the rate-determining step which is preceded by fast proton transfer equilibrium (K_a). The time evolution of the concentration of the low-pH form (P_AH) in eq 13 would be given as

$$[P_AH] = [P_AH]_f - ([P_AH]_f - [P_AH]'_f) \times \exp\left[-\left(k_4 + \frac{K_a(k_3 + k_4)}{[H^+]_f}\right)t\right] \quad (14)$$

where $[P_AH]'_f$ is the concentration of the low-pH form at the final pH (pH_f) at $t = 0$, i.e., before the onset of the conformational transition (step 2). The apparent rate constant in eq 13 would thus be

$$k_{app} = k_4 + \frac{K_a(k_3 + k_4)}{[H^+]_f} \quad (15)$$

A plot of the experimental k_{app} against pH is shown in the lower panel of Figure 9. The solid line through the data shows the best fit to eq 12 ($[H^+]$ in eq 12 is written as 10^{-pH}), and the inset in the lower panel of Figure 9 shows the linear fit to k_{app} against $[H^+]$ (eq 12). The experimental k_{app} values could not be fitted to eq 15. Thus the present results support eq 10a,b as the mechanism of the pH-induced conformational transition in PdII. The values of the parameters k_1 and $k_2/(1 + K_{iso})$ calculated from the fit to the experimental k_{app} against pH by eq 12 were found to be $k_1 = 0.029 \pm 0.005\ s^{-1}$ and $k_2/(1 + K_{iso}) = (1.7 \pm 0.05) \times 10^6\ M^{-1}\ s^{-1}$.

The rate of deprotonation of amino acids in aqueous medium is generally a diffusion-controlled process (*36*) while that inside the protein matrix could become very slow depending on the nature of the surrounding environment. The crystal structure of PdII (Figure 1) showed that the coordinated residues C216, E218, C220, H224, and M227 belong to the loop joining β9 and β10 while H181 belongs to the loop joining β5 and β6. The H224 residue is exposed to the solvent. The protein has a β-barrel (Greek key type) topology (*25*), which is stabilized by hydrophobic interactions of the nonpolar side chains. The sheets are also connected through inter-sheet hydrogen-bonding (*8*, *33*) interactions. The inter-sheet hydrogen-bonding network may be formed by polar aromatic amino acid residues such as tyrosines and tryptophans directed toward the core of the β-barrel. The crystal structure shows (Figure 1) that the polar side chains of Tyr125 and Tyr127 are directed toward the core of the β-barrel. The crystal structure also shows the presence of a water molecule inside this core of the β-barrel, which is 2.5 Å away from the hydroxyl group of Tyr125. This indicates that the core of the β-barrel possibly contains a hydrogen-bonding network involving the Tyr125 and water. Deprotonation of the Tyr 125 residue at high pH would thus possibly decrease the stability of the β-barrel and lead to a conformational change in the protein in this region. It may thus be proposed that the high-pH species of the protein is formed due to deprotonation of the Tyr125 residue leading to a small conformational change in the β-barrel which causes changes in the geometry of the dicopper center. Deprotonation of the other tyrosine residue (Tyr127) may also cause a similar change. The results thus indicate that the tyrosine residue (possibly Tyr125 or Tyr127) buried in the hydrophobic core of the protein might be deprotonated with $pK_a = 8.2$, which would lead to breaking of the associated hydrogen-bonding network of PdII at high pH. This subsequently may cause a change in the conformation of the β-barrel leading to breaking or weakening of the H224 coordination to copper which gives rise to the formation of the high-pH form.

Deprotonation of the tyrosine residue in the hydrophobic region would be associated with a smaller rate constant possibly because of slow diffusion of protons into the hydrophobic pocket of the protein. The subsequent conformational change in the β-barrel is triggered by breaking of the hydrogen-bonding network at high pH, and this process would be very fast.

CONCLUSIONS

An increase in pH was found to cause conformational changes in the CuA site of PdII of *P. denitrificans*. UV−visible spectral studies showed an increase in the intensity of the 360 nm absorption band with a subsequent decrease in absorption bands at 480, 535, and 810 nm with increase in pH. CD spectral studies also showed an increase in the ellipticity of the 365 and 522 nm bands with a subsequent decrease in the ellipticity of the 333 and 443 nm bands with increase in pH. These changes in spectral features arise due to a change in the conformation of the binuclear CuA site of the protein. The low-pH and high-pH forms were shown to exist in thermal equilibrium at ambient pH, and an increase in temperature caused conversion of the low-pH form to the high-pH form. The pK_a for the equilibrium was found to be 8.2, which possibly corresponds to deprotonation of a tyrosine residue in the protein. The low-pH species was found to be more stable compared to the high-pH species as indicated by thermal unfolding and urea-induced unfolding studies. The results suggested that deprotonation of the Tyr125 or Tyr127 may cause a drastic change in the conformation of the copper site, which might be responsible for breaking or weakening of the H224 ligation to the copper. Stopped-flow kinetic studies showed that the rate-determining step for the conformational transition involves deprotonation of the tyrosine residue, which is followed by a fast conformational transition from the low-pH to the high-pH form.

The pH-induced conformational change of the dicopper site observed in the present case might have some implication in the biochemical function of the intact cytochrome oxidase. The CuA acts as the electron entry site in the enzyme (*1*−*3*), and hence the pH-induced conformational change in this site could act as a gating mechanism to the respiratory electron transfer in CcO. The isolated subunit II of cytochrome oxidase, however, seems to have structural properties different from those in the intact enzyme (*13*). Thus the present results could not directly be correlated to the properties of the intact enzyme. However, the present results highlighted that the pH-induced conformational transition at the dicopper center could indeed be a candidate for the gating

mechanism in the intact enzyme, which needs to be explored by further studies on the enzyme itself.

ACKNOWLEDGMENT

The authors thank Mr. B. T. Kansara for help.

REFERENCES

1. Saraste, M. (1990) *Q. Rev. Biophys. 23*, 331−336.
2. Wikstrom, M., Krab, K., and Saraste, M. (1981) in *Cytochrome Oxidase A Synthesis*, Academic Press, New York.
3. Saraste, M. (1999) *Science 283*, 1488−1493.
4. Tsukihara, T., Aoyama, H., Yamashita, E., Tomizaki, T., Yamaguchi, H., Shinzawa-Itoh, K., Nakashima, R., Yaono, R., and Yoshikawa, S. (1996) *Science 272*, 1136−1144.
5. Wikstrom, E., Ed. (1998) Minireview Series: Cytochrome Oxidase: Structure and Mechanism, *Journal of Bioenergetics and Biomembranes*, Vol. 30, Plenum, New York.
6. Wilmanns, M., Lappalainen, P., Kelly, M., Sauer-Eriksson, E., and Saraste, M. (1995) *Proc. Natl. Acad. Sci. U.S.A. 92*, 11955−11959.
7. Williamss, P. A., Blackburn, N. J., Sanders, D., Bellamy, H., Stura, E. A., Fee, J. A., and McRee, D. E. (1999) *Nat. Struct. Biol. 6*, 509−516.
8. Ostermeier, C., Harrenga, A., Ermler, U., and Michel, H. (1997) *Proc. Natl. Acad. Sci. U.S.A. 94*, 10547−10553.
9. Iwata, S., Ostermeier, C., Ludwig, B., and Michel, H. (1995) *Nature 376*, 660−669.
10. Zumft, W. G., and Kroneck, P. M. H. (1996) *Adv. Inorg. Biochem. 11*, 193−221.
11. Sykes, A. G. (1991) *Adv. Inorg. Chem. 36*, 175−408.
12. Farrar, A. J., Lappalainen, P., Zumft, W. G., Saraste, M., and Thomson, A. J. (1995) *Eur. J. Biochem. 232*, 294−303.
13. Lappalainen, P., Asas, R., Malmstrom, B. G., and Saraste, M. (1993) *J. Biol. Chem. 268*, 26416−26421.
14. Blackburn, N. J., Barr, M. E., Woodruff, W. H., van der Ooost, J., and de Vries, S. (1994) *Biochemistry 33*, 10401−10407.
15. Dennison, C., Berg, A., de Vries, S., and Canters, G. W. (1996) *FEBS Lett. 394*, 340−344.
16. Slutter, C. E., Sanders, D., Wittumg, P., Malmstrom, B. G., Asa, R., Richards, J. H., Gray, H. B., and Fee, J. A. (1996) *Biochemistry 35*, 3387−3395.
17. Salgado, J., Warmerdam, G., Bubacco, L., and Canters, W. (1998) *Biochemistry 37*, 7378−7389.
18. Oost, J., Lappalainen, P., Musacchio, A., Warne, A., Lemienux, L., Rumbley, J., Gennis, R. B., Aasa, R., Pascher, T., Malmstrom, B. G., and Sarate, M. (1992) *EMBO J. 11*, 3209−3217.
19. Hay, M. T., Ang, M. C., Gamalin, D. R., Solomon, E. I., Antholine, W. E., Ralle, M., Blackburn, N. J., Wang, M. X., Kwon, A. H., and Lu. Y. (1998) *Inorg. Chem. 37*, 191−198.
20. Hay, M., Richards, J. H., and Lu, Y. (1996) *Proc. Natl. Acad. Sci. U.S.A. 93*, 461−464.
21. Luchinat, C., Soriano, A., Djinovic-Carugo, K., Saraste, M., Malmstrom, B. G., and Bertini, I. (1997) *J. Am. Chem. Soc. 119*, 11023−11027.
22. Farrar, A. J., Neese, F., Lappalainen, P., Kroneck, P. M. H., Saraste, M., Zumft, W. G., and Thomson, A. J. (1996) *J. Am. Chem. Soc. 118*, 11501−11514.
23. Farver, O., Lu, Y., Ang, M. C., and Pecht, I. (1999) *Proc. Natl. Acad. Sci. U.S.A. 96*, 899−902.
24. Lappalainen, P., Watmough, N. J., Greenwood, C., and Saraste, M. (1995) *Biochemistry 34*, 5824−5830.
25. Wittung, P., Kallebring, B., and Malmstrom, B. G. (1994) *FEBS Lett. 349*, 286−288.
26. Holm, L., Saraste, M., and Wikstrom, M. (1987) *EMBO J. 6*, 2819−2823.
27. Pace, C. N. (1996) *Methods Enzymol. 131*, 266−280.
28. Bolen, D. W., and Santoro, M. M. (1988) *Biochemistry 27*, 8069−8074.
29. Wittung-Stafshede, P., Malmstrom, B. G., Sanders, D., Fee, J. A., Winkler, J. R., and Gray, H. B. (1998) *Biochemistry 37*, 3172−3177.
30. Bohm, G., Muhr, R., and Jaenicke, R. (1992) *Protein Eng. 5*, 191.
31. Winkler, J. R., Wittung-Stafshede, P., Leckner, J., Malmstrom, B. G., and Gray, H. B. (1997) *Proc. Natl. Acad. Sci. U.S.A. 94*, 4246−4249.
32. Pascher, T., Chesick, J. P., Winkler, J. R., and Gray, H. B. (1996) *Science 271*, 1558−1560.
33. Robinson, H., Ang, M. C., Gao, Y., Hay, M. T., Lu, Y., and Wang, A. H. (1999) *Biochemistry 38*, 5677−5683.
34. Gamelin, D. R., Randall, W, D., Hay, M. T., Houser, R. P., Mulder, T. C., Canters, G. W., de Vries, S., Tolman, W. B., Lu, Y., and Solomon, E. I. (1998) *J. Am. Chem. Soc. 120*, 5246−5263.
35. Leckner, J., Wittung, P., Bonander, N., Karlsson, B. G., and Malmstrom, B. G. (1997) *J. Biol. Inorg. Chem. 2*, 368−371.
36. Fersht, A. (1977) in *Enzyme Structure and Mechanism*, 2nd ed., Chapter 4, W. H. Freeman and Co., New York.

BI002212E